Continuous-flow crystallisation in 3D-printed compact devices – Supporting information

Obinna Okafor,[a] Karen Robertson,[a] Ruth Goodridge[a] and Victor Sans*[a,b]

1. *Temperature acquisition system*

An acquisition system for in-situ monitoring of the temperature in flow was designed. This served as a cost-effective method of monitoring the temperature at different points in the reactor. K-type thermocouples where attached to 1/16" tube connectors with araldite glue. The thermocouples were then coupled with an MAX6675 thermocouple sensor module which was linked to an Arduino mega micro-controller. Temperature was collected per second. The schematic and setup of the temperature acquisition system is presented in Figure S1. Labview was used to compile the data received from the Arduino software linked to the micro-controller.

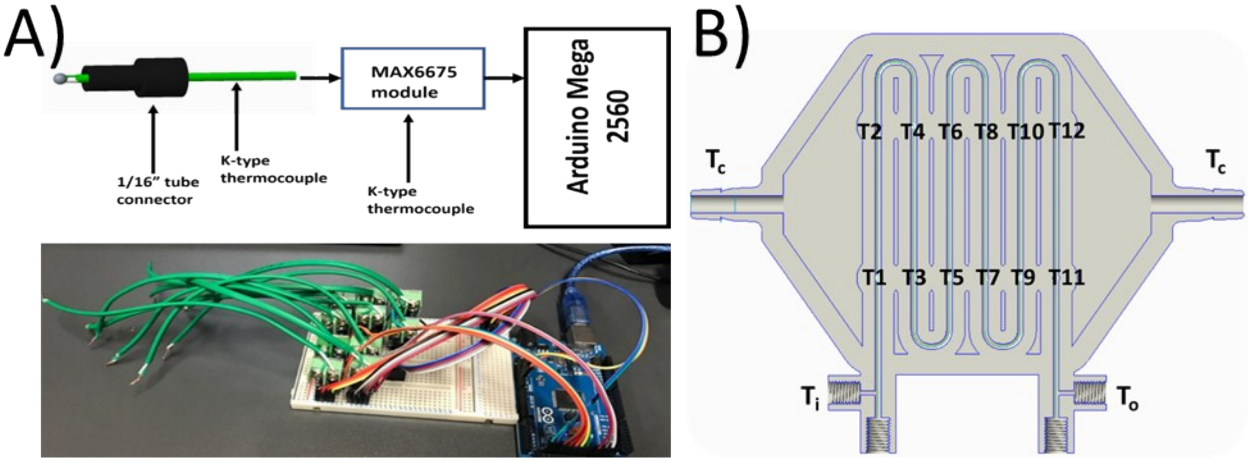

Figure S1: A) (Top) Schematic of inline temperature acquisition system and (below) actual setup. B) Schematic representation of the distribution of the thermocouples in the crystalliser.

2. *Design of experiments*

Deducing the change in temperature across the reactor, from the inlet to outlet is crucial, as this will allow the modelling of the thermal behaviour of the device. As the designed device will also behave uniquely at different flow rates, temperatures and dissimilar materials, experiments were carried out enveloping the varying parameter changes. The following heat transfer experiments were carried out on the crystalliser Agu II.I:

- Heating of the heat transfer chamber between 40°C to 25°C at a constant flow rate of 0.5ml/min at inlet temperature of 23°C to 25°C.

- Heating of the heat transfer chamber between 20°C to 5°C at a constant flow rate of 0.5ml/min and inlet temperature of 23°C to 24°C.

- Flow rate change of the reactor chamber between 0.25ml/min to 2ml/min at a constant chiller temperature of 5°C and inlet temperature of 24°C.
- Flow rate change of the reactor chamber between 0.1ml/min to 3ml/min at a constant chiller temperature of 40°C and inlet temperature of 24°C.

Table S1: Design of experiments to characterise heat transfer in Agu II.I at varying flow rates and chiller temperature.

Code	Reactor flow rate	Chiller Temp.	Comments
H1	0.5ml/min	25°C	Heating at constant flow rate.
H2	0.5ml/min	30°C	Heating at constant flow rate.
H3	0.5ml/min	35°C	Heating at constant flow rate.
H4	0.5ml/min	40°C	Heating at constant flow rate.
C1	0.5ml/min	23°C	Cooling at constant flow rate.
C2	0.5ml/min	20°C	Cooling at constant flow rate.
C3	0.5ml/min	15°C	Cooling at constant flow rate.
C4	0.5ml/min	10°C	Cooling at constant flow rate.
C5	0.5ml/min	5°C	Cooling at constant flow rate.
FC1	2.0ml/min	5°C	Varying flow rates at constant cooling.
FC2	1.5ml/min	5°C	Varying flow rates at constant cooling.
FC3	1.0ml/min	5°C	Varying flow rates at constant cooling.
FC4	0.5ml/min	5°C	Varying flow rates at constant cooling.
FC5	0.25ml/min	5°C	Varying flow rates at constant cooling.
FH1	3.0ml/min	40°C	Varying flow rates at constant heating.
FH2	2.0ml/min	40°C	Varying flow rates at constant heating.
FH3	1.5ml/min	40°C	Varying flow rates at constant heating.
FH4	0.5ml/min	40°C	Varying flow rates at constant heating.
FH5	0.5ml/min	40°C	Varying flow rates at constant heating.
FH6	0.5ml/min	40°C	Varying flow rates at constant heating.
FH7	0.5ml/min	40°C	Varying flow rates at constant heating.

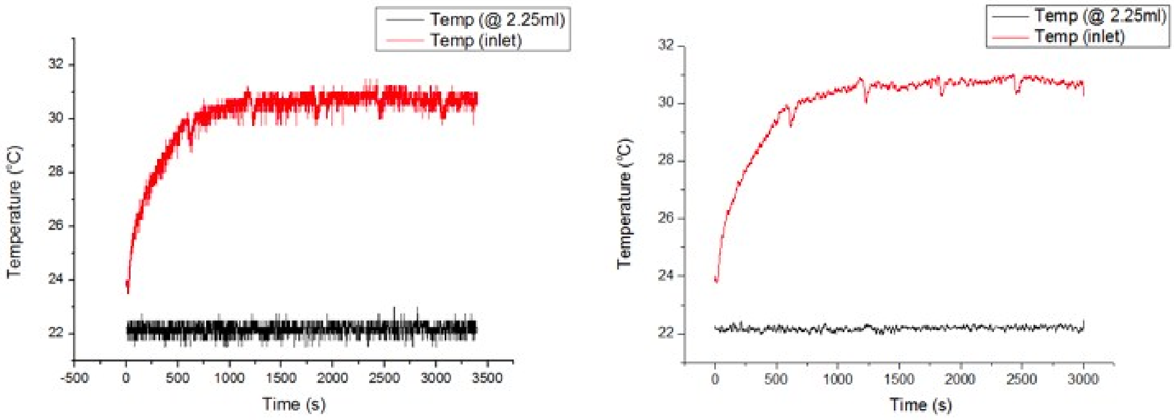

Figure S2: Noise observed in the temperature data. Temperature at 2.5ml from the inlet of the reactor is shown in the red line, while the black line is the temperature at the inlet of the reactor. (left) The raw collected data, (right) smoothed employing a 10-point fast Fourier transform (FFT) algorithm. The chiller temperature was set to 20°C. The flow through the reactor can be seen to achieve steady state in about 25mins.

3. *Heat transfer Modelling*

The modelling carried out in this work was simplified by assuming the following:

- Temperature at the internal wall surface is assumed constant across the tube length. This is not the case however, because some parts of the tube wall are attached to the wall of the crystalliser. Also, some of the support structure is densely populated at the lower regions of the crystalliser, which will result in an unevenly distributed flow across the tubes.
- There is no loss or drop in temperature in the heat transfer chamber. However, it is expected that there will be a drop in temperature to the surroundings of the recirculating fluid from the inlet to the outlet.
- The flow rate of both fluids are assumed to be constant.
- The temperature sensors are positioned in the flow path of the fluid without any dead zones.
- The temperature of the circulating fluid is constant during each experiment.
- Steady state was achieved before data was collected.

Modelling of the collected data was carried out using the following heat transfer equation:

$$\frac{T_s - T_{m,o}}{T_s - T_{m,i}} = exp\left[-\frac{PLU}{mc_p}\right] \quad \text{E1}$$

$$U = \left(\frac{1}{h_i} + \frac{1}{h_o}\right)^{-1} \quad \text{E2}$$

$$h = \frac{Nu.k}{D_h} \quad \text{E3}$$

$$Nu = 0.023.\,Re^{0.8}\left(\frac{\mu c_p}{k}\right)^{0.3} \quad \text{E4}$$

Where T_s is the temperature at the tube internal surface, $T_{m,i}$ and $T_{m,o}$ represents the temperature at the middle inlet and outlet of the tube. P is the perimeter, L is the tube length, m is the mass flow rate, μ is the dynamic viscosity, k is the thermal conductivity, Re is the Reynold number, U is the overall heat transfer coefficient, c_p is the heat capacity of the fluid, h_i and h_o are the convective heat transfer coefficient of the internal and external fluid. Nu corresponds to the Nusselt number. Nu value of 3.66 was used for the hi calculation, an approximation for fully developed laminar flow, while equation 4 was used for Nu_o calculation. For modelling purposes, the equation was simplified by assuming a linear relation between the outside temperature in the heat transfer chamber T_∞ and the internal surface temperature.

$$T_{m,o} = A.T_\infty - [A.T_\infty - T_{m,i}].exp\left[-\frac{PLU}{mcp}\right] \quad \text{E3}$$

$$Q = \frac{2\pi k}{\ln\left({r_2}/{r_1}\right)}.(T_1 - T_2) = \frac{2\pi k}{\ln\left({r}/{r_1}\right)}.(T_1 - T) \quad \text{E4}$$

Effect of change in wall thickness and material

To compare the differences in temperature profile as a factor of the wall thickness the fitted models for the highest and lowest temperatures measures were used. The models for the case of the chiller temperature at 40^{o}C (heating) and 5^{o}C (cooling) were modelled for a wall/tube thickness of 0.45mm to 5.45mm. The thickness of the tubes used in the experiments was 3.45mm.

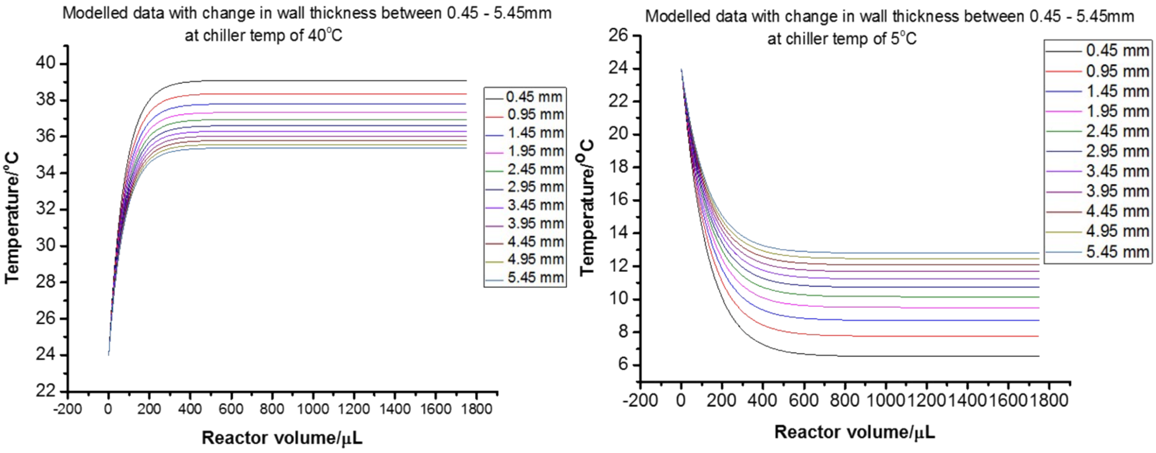

Figure S3: Modelled data for changes in wall thickness with change in thickness between 0.45-5.45mm. At chiller temperature of 5-40^{o}C.

From the model, it is observed that increasing the thickness of the wall increases the resistance to heat transfer. Hence, a less steep temperature drop can be achieved with the increase in wall thickness and vice versa. Similar results can be seen and both cooling and heating. This however represents the case of an ideal system. In a real and more representative system, inconsistences in the fabricated material and non-homogeneous parts or faces in contact with the fluid will have an effect on the heat transfer between the fluids.

The acrylate based AM resin poses a suitable material for studies in the recrystallization of paracetamol for several reasons: It is found to have a good resistivity to a range of solvents including Isopropanol which is used in this work. Secondly, the material is found to have a stable thermal conductivity in the range of temperatures tested. Hence an indication that the material is stable in the range of temperatures. This is observed by plotting the modelled reactant side temperature to the actual chiller side temperature, Figure 3.

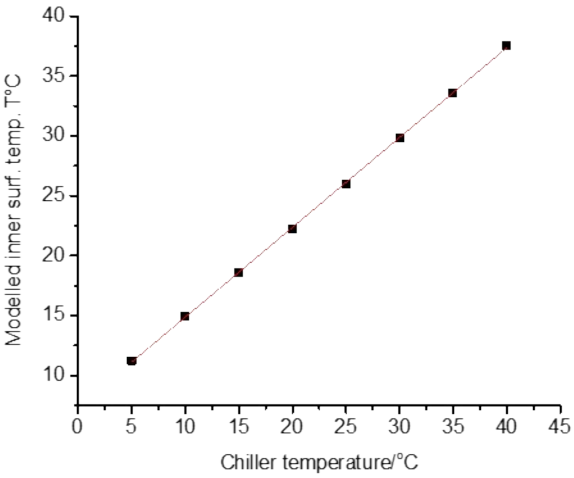

Figure S4: Modelled reactant side temperature and the actual reactant side temperature.

Cooling crystallisation in the AM material also provides the benefit of a less steep temperature gradient compared to traditional materials used in flow reactors. Flow reactor and crystallisers are commonly manufactured in glass or metallic materials with higher thermal conductivity values. For comparison, a temperature profile of the ideal crystalliser behaviour with a measured thermal conductivity of 0.4W/mK compared with Aluminium at 205W/mK and glass at 1.05W/mK. The profiles at 40^{o}C and 5^{o}C in can be seen to have a steeper gradient in the AM material. The less steep gradient of temperature in crystallisation will aid in minimising fouling and uneven crystal size distribution associated with rapid drop in temperature.

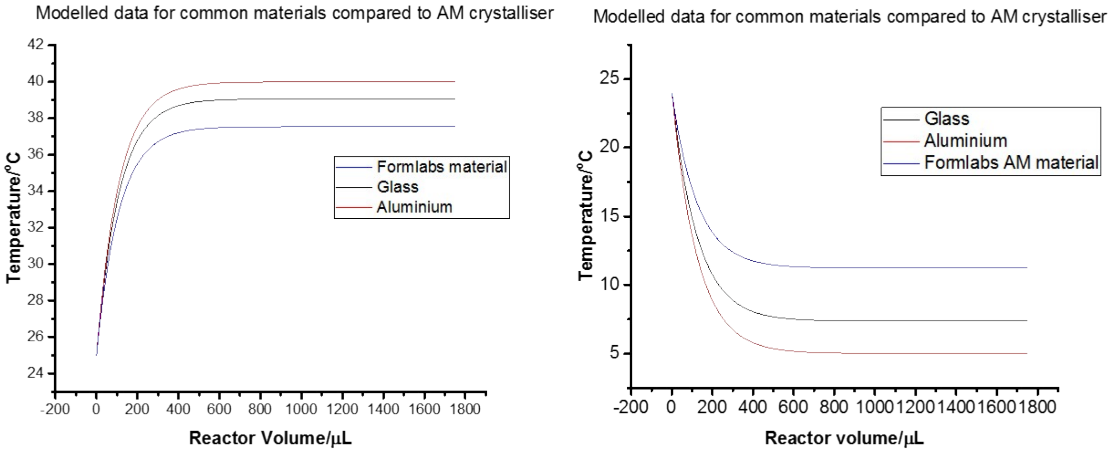

Figure S5: Modelled data for temperature profile in the crystalliser compared to a similar crystalliser fabricated in glass and aluminium. At chiller temperature of 40^{o}C (left) and 5^{o}C (right)

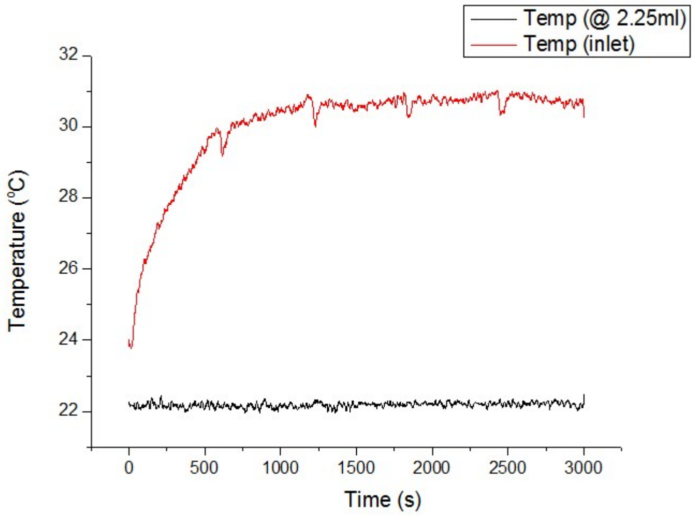

Figure S6: Deeps in temperature observed during refill. (black) Temperature at inlet of crystalliser. (red) Temperature at 2.25mL into the reactor, close to the mid-section.

Thermal conductivity measurement

The thermal conductivity of the cured resin used in the manufacture of the reactors was characterised. The thermal conductivity measurement allowed the quantifying of the heat transfer rate between the chiller and the reactant fluid. For this purpose, three 15mm OD cylinders with varying thickness of 3, 4 and 5mm were fabricated on the Form 2 device. The thermal conductivity measurements were carried out on a TCi Thermal Conductivity Analyzer utilising a Modified transient plane source (MTPS) sensor. The device employs a one-sided interfacial heat sensor that applies a heat to the sample and measures the thermal conductivity of the material. This is done by inducing a one-dimensional heating to the sensor and material resulting in a rise in temperature by an applied current. The applied current induces a change in the voltage drop in the sensor. Heat generated dissipates into the sample and the rate depends on the transport properties of the material. The rate of increase in voltage, which is calibrated to the temperature, is inversely proportional to the thermal conductivity. Hence, the slope for highly conductive materials will be flatter, while steeper in materials with lower conductivity.
Two of the three-cylinder thicknesses were fabricated and tested. 10 measurements were collected for each of the samples and the averages are presented.

Table S2: Determination of thermal conductivity values for different cylinder thicknesses.

Cylinder thickness (mm)		**effusivity** (w $s^{½}$ m^{-2} k^{-1})	**k** (w m^{-1} k^{-1})
5	part 1	744.76	0.37
	part 2	770.22	0.39
4	part 1	797.25	0.42
	part 2	895.61	0.52
3	part 1	854.05	0.47
	part 2	917.96	0.54

Although the MTPS measurement is a surface technique and the thermal conductivity of the material should not relate to the thickness of the material, variations in the measurement was found. This could be either due to the uneven density of the fabricated material or errors in the measuring devices. Variations can also arise for surface roughness variation of the materials resulting in varying contact surfaces or the packing structure of the polymer. The measurements were however found to be in the range of +/-0.09W/mK at a mean thermal conductivity of 0.45 W/mK. The thermal conductivity measurement was plugged into the heat transfer model to predict the effect of change in thickness of the material.

4. *Crystallisation study*

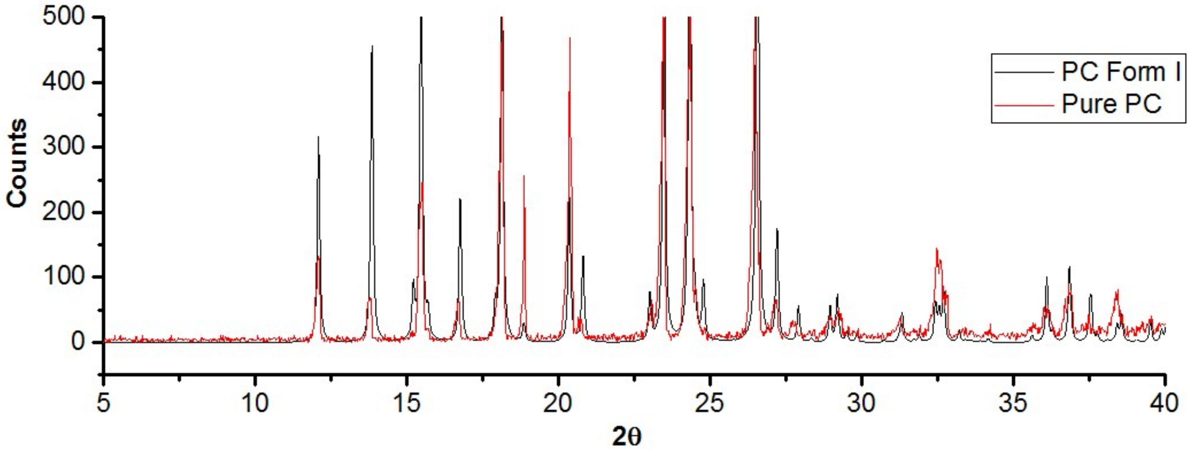

Figure S7: Diffractogram of Paracetamol (PC) purchased from Sigma Aldirch overlaid with PC Form I reference data. It can be seen to closely match.

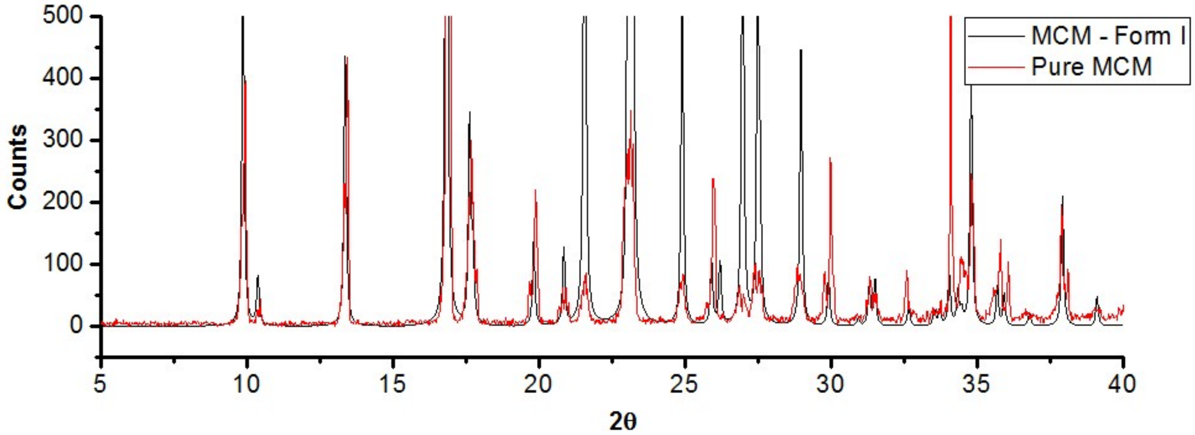

Figure S8: Diffractogram of Metacetamol (MCM) purchased from Sigma Aldirch overlaid with MCM reference data. It can be seen to closely match.

Table S3: PC crystallisation experiments. Showing flow rate jacket temp and material collection interval.

First run

Flow rate (ml/min)	Temp (^oC)	Time (mins)
0.5	5	20

0.5	10	20
0.5	15	20
0.5	25	20
0.5	30	20
Second run		
Flow rate (ml/min)	Temp (^{o}C)	Time (mins)
0.5	10	10
0.5	10	30
0.5	10	60
0.5	0	10
0.5	0	30
0.5	0	60
0.5	5	10
0.5	5	30
0.5	5	60

5. Diffractograms

The diffractograms for the collected samples are plotted against CSD reference HXACAN01 – PC monoclinic form I, HXACAN26 - PC orthorhombic form II and MENSEE – MCM form I Comparison in the order of Table S3. The powder particles from the first run were collected after 20mins, while the on the second run, they were collected at intervals of 10, 30 and 60 mins (denoted as T10, T30 and T60 on the plots).

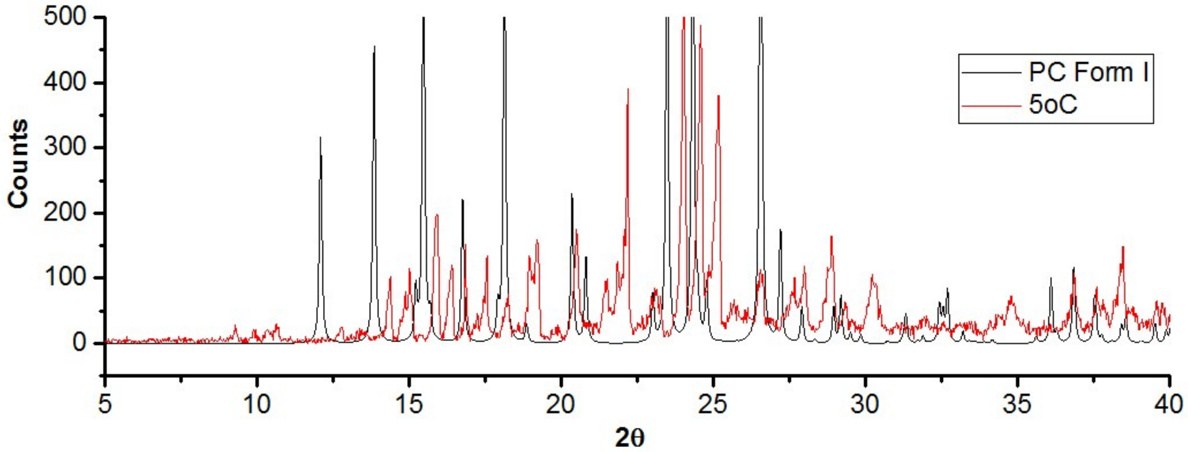

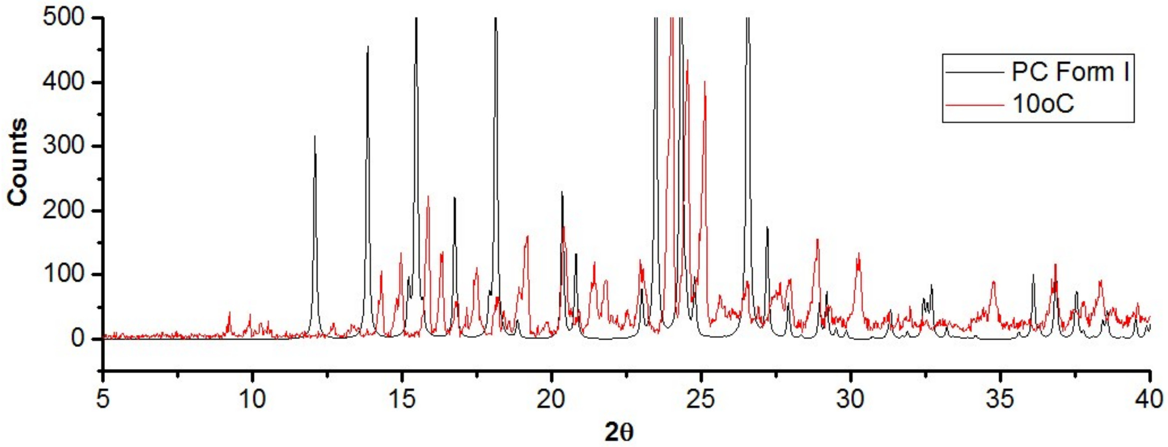

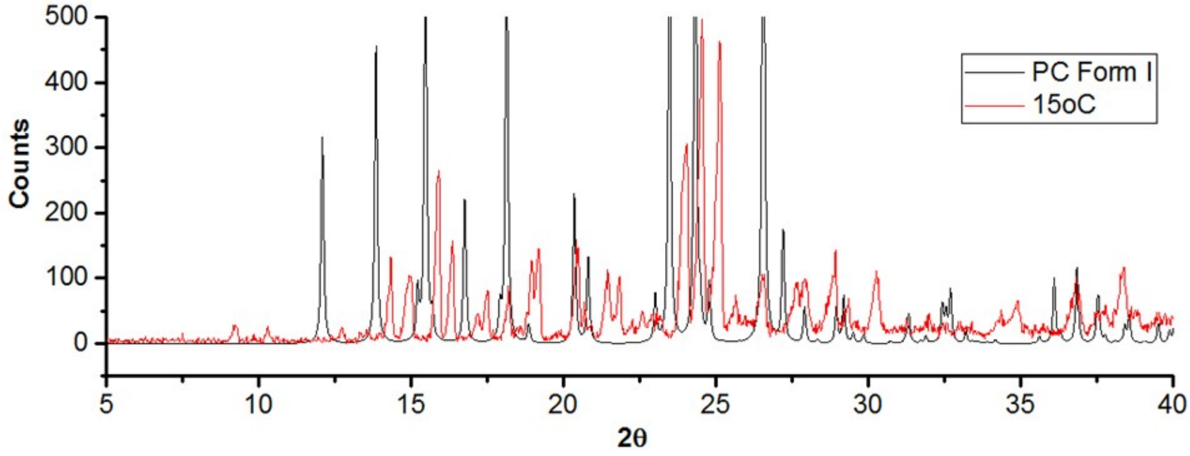
Counts
500
400
300
200
100
0
5
10
15
20
25
30
35
40
2θ
PC Form I
15oC

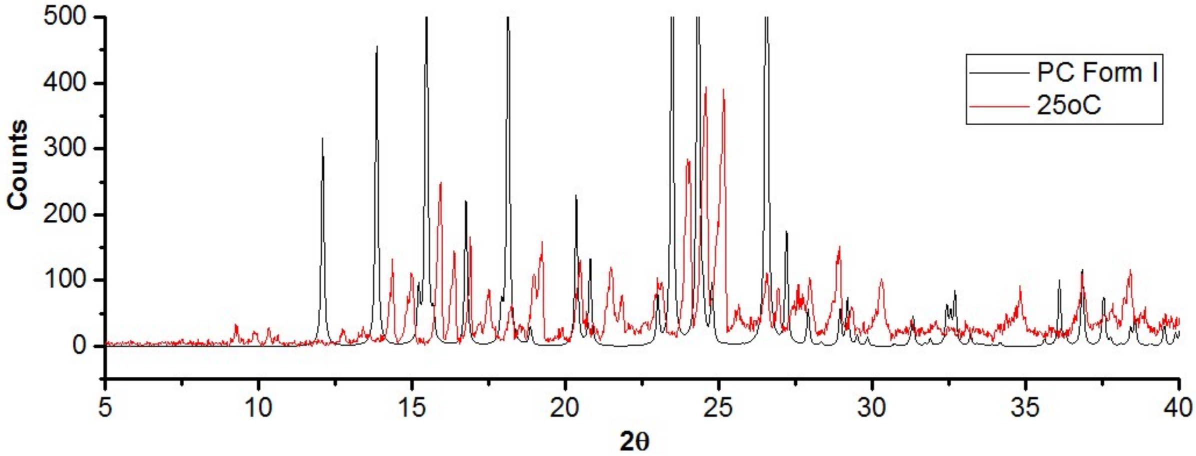
Counts
500
400
300
200
100
0
5
10
15
20
25
30
35
40
2θ
PC Form I
25oC

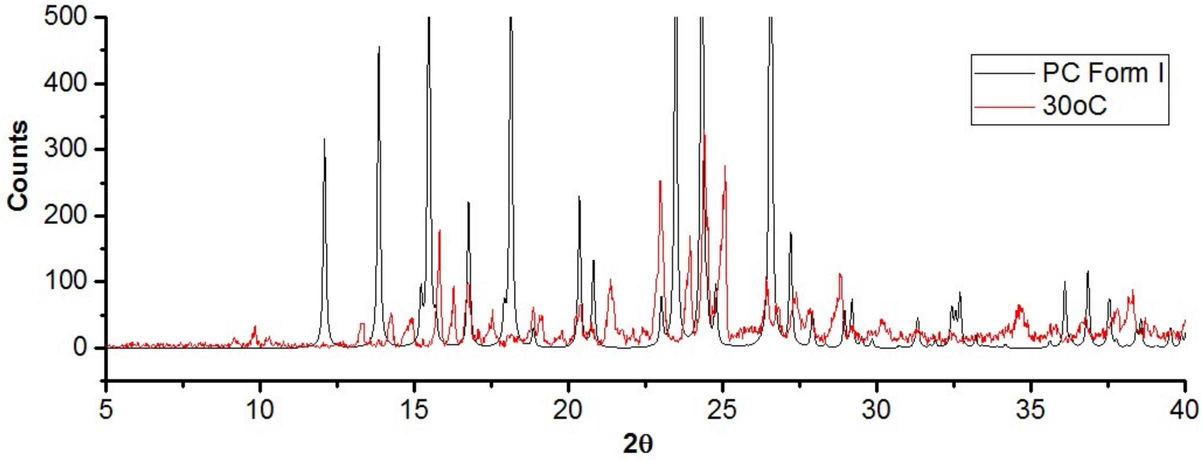
Counts
500
400
300
200
100
0
5
10
15
20
25
30
35
40
2θ
PC Form I
30oC

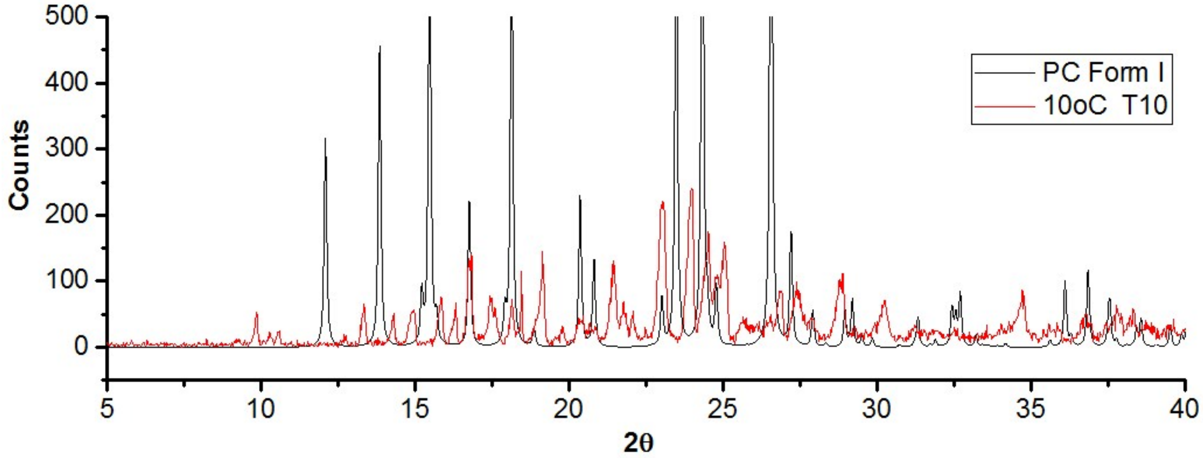
PC Form I
10oC T10
Counts
500
400
300
200
100
0
5
10
15
20
25
30
35
40
2θ

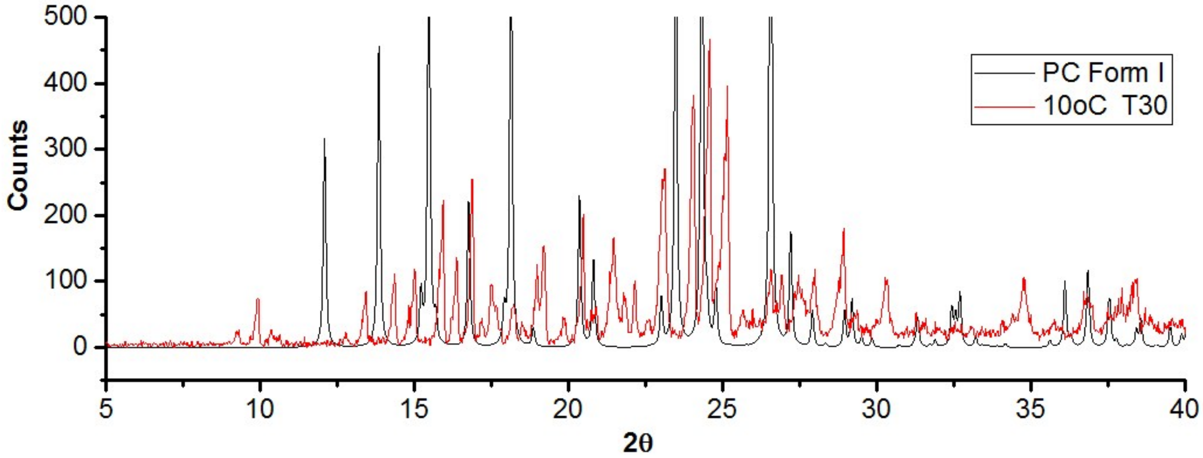
PC Form I
10oC T30
Counts
500
400
300
200
100
0
5
10
15
20
25
30
35
40
2θ

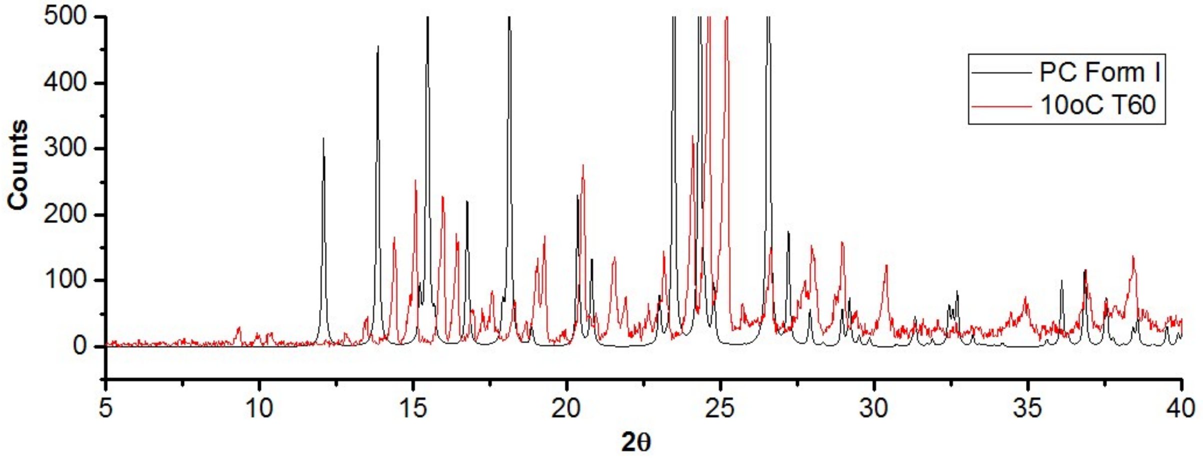
PC Form I
10oC T60
Counts
500
400
300
200
100
0
5
10
15
20
25
30
35
40
2θ

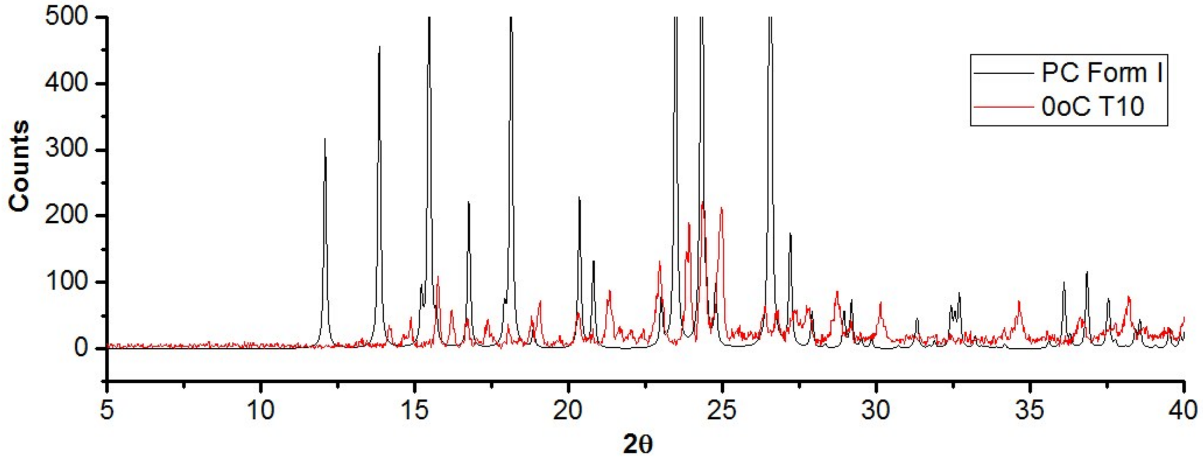
Counts
500
400
300
200
100
0
5
10
15
20
25
30
35
40
2θ
PC Form I
0oC T10

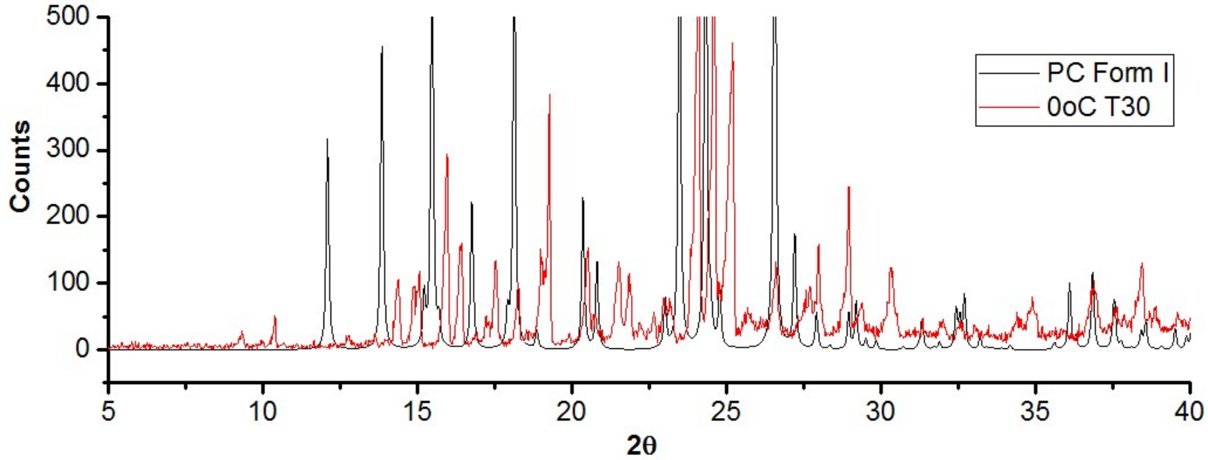
Counts
500
400
300
200
100
0
5
10
15
20
25
30
35
40
2θ
PC Form I
0oC T30

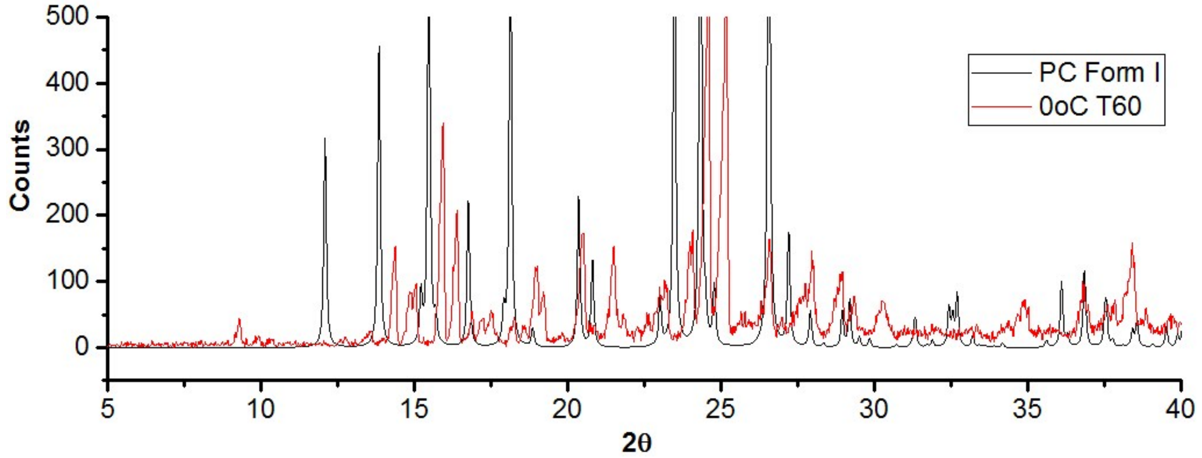
Counts
500
400
300
200
100
0
5
10
15
20
25
30
35
40
2θ
PC Form I
0oC T60

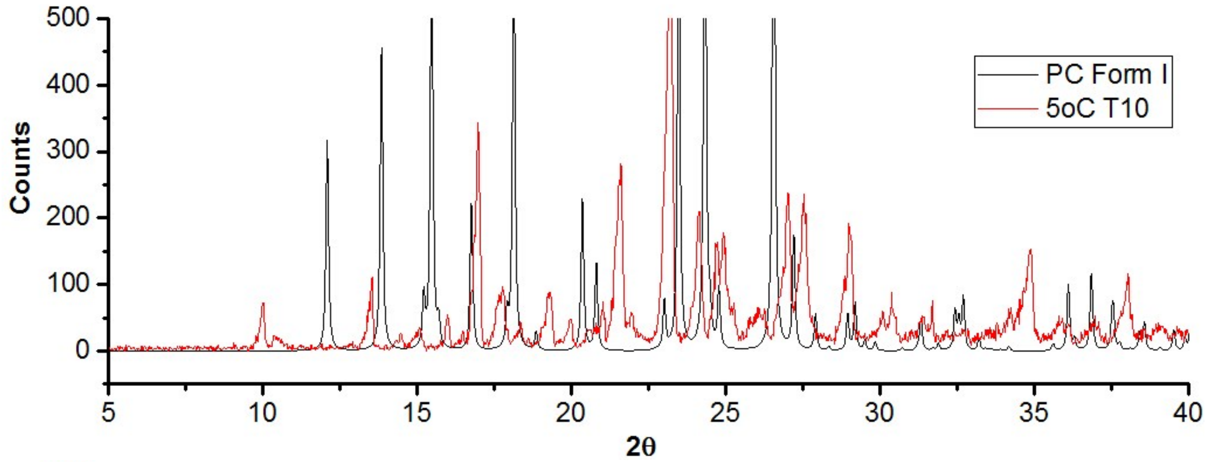
Counts
500
400
300
200
100
0
5
10
15
20
25
30
35
40
2θ
PC Form I
5oC T10

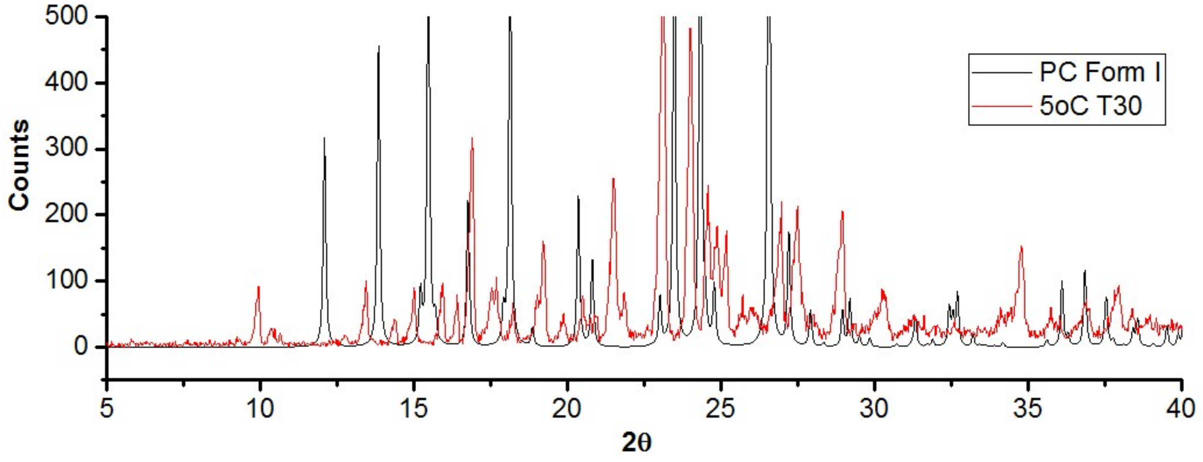
Counts
500
400
300
200
100
0
5
10
15
20
25
30
35
40
2θ
PC Form I
5oC T30

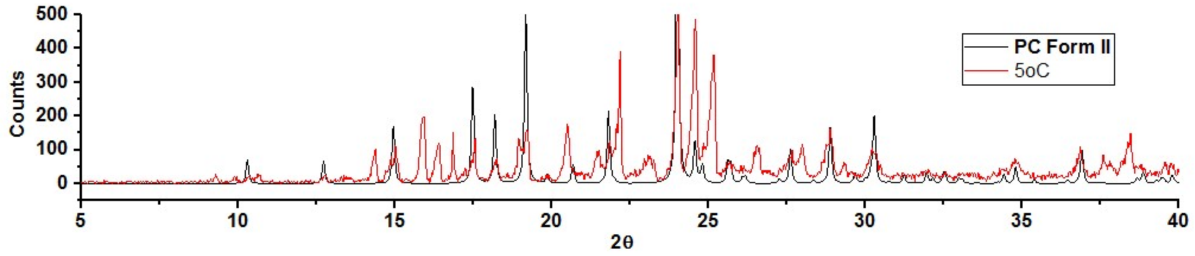
Counts
500
400
300
200
100
0
5
10
15
20
25
30
35
40
2θ
PC Form II
5oC

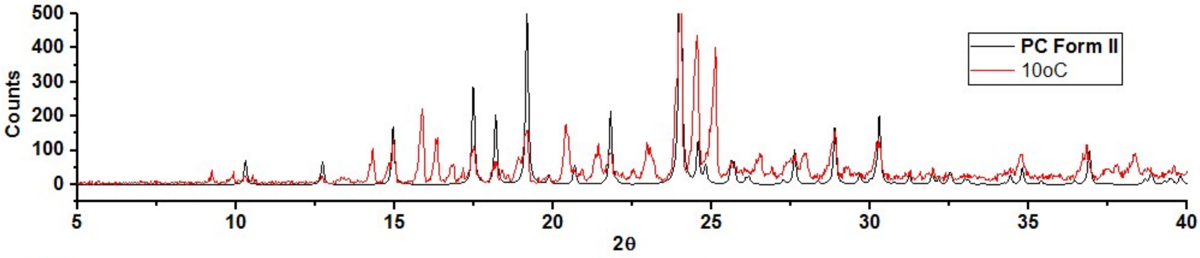
Counts
500
400
300
200
100
0
5
10
15
20
25
30
35
40
2θ
PC Form II
10oC

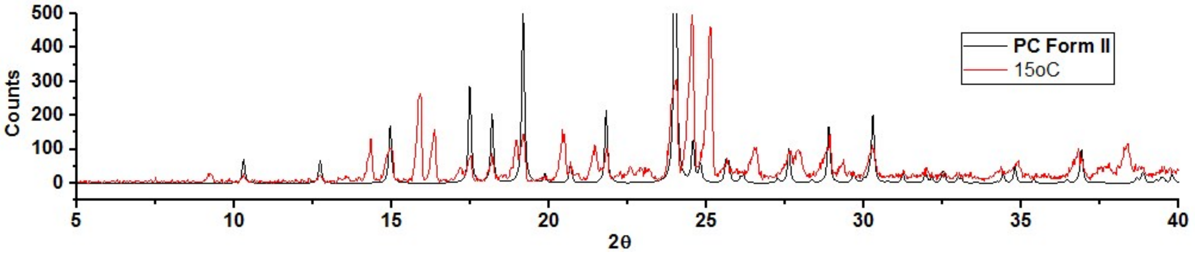
Counts
500
400
300
200
100
0
5
10
15
20
25
30
35
40
2θ
PC Form II
15oC

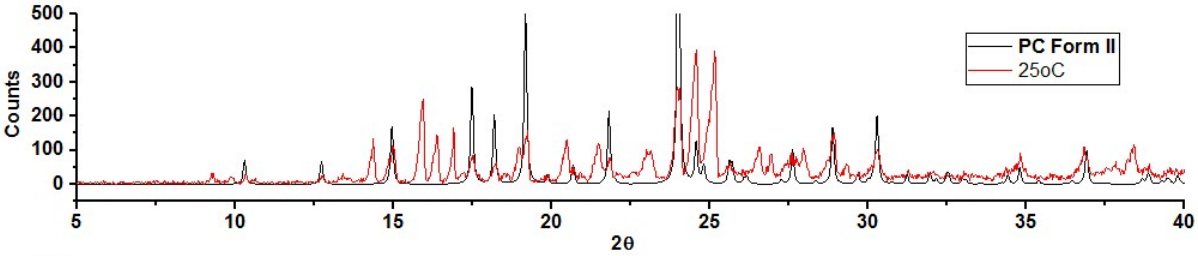
Counts
500
400
300
200
100
0
5
10
15
20
25
30
35
40
2θ
PC Form II
25oC

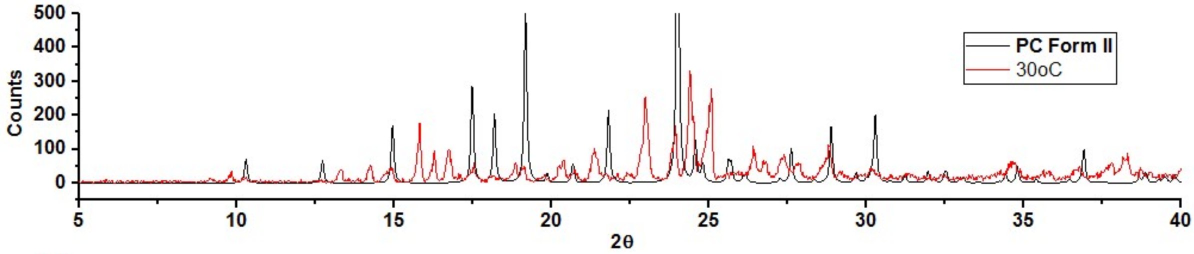
Counts
500
400
300
200
100
0
5
10
15
20
25
30
35
40
2θ
PC Form II
30oC

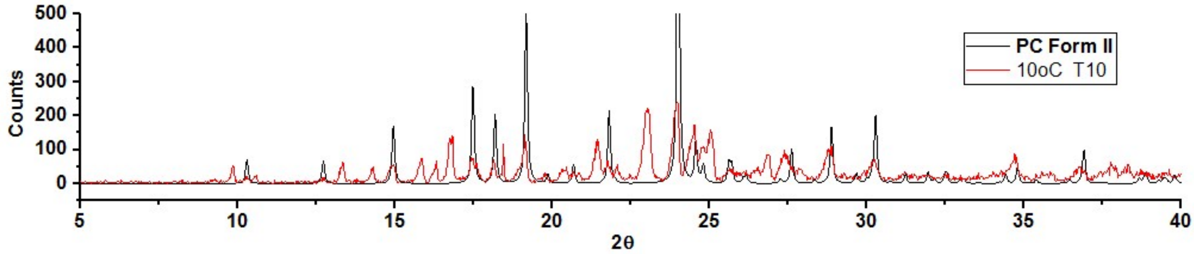
Counts
500
400
300
200
100
0
5
10
15
20
25
30
35
40
2θ
PC Form II
10oC T10

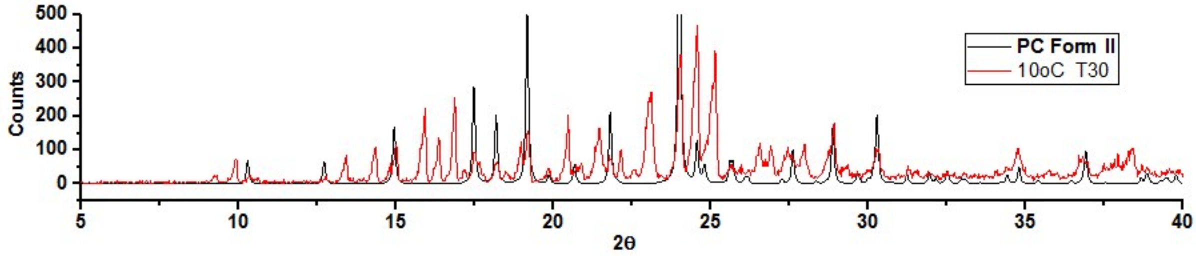
Counts
500
400
300
200
100
0
5
10
15
20
25
30
35
40
2θ
PC Form II
10oC T30

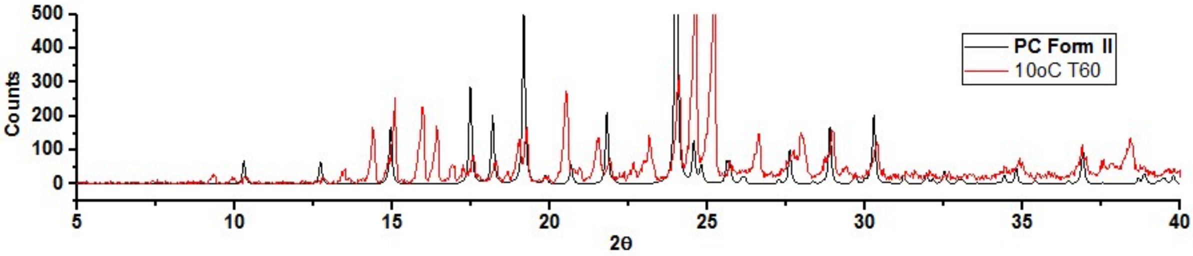
Counts
500
400
300
200
100
0
5
10
15
20
25
30
35
40
2θ
PC Form II
10oC T60

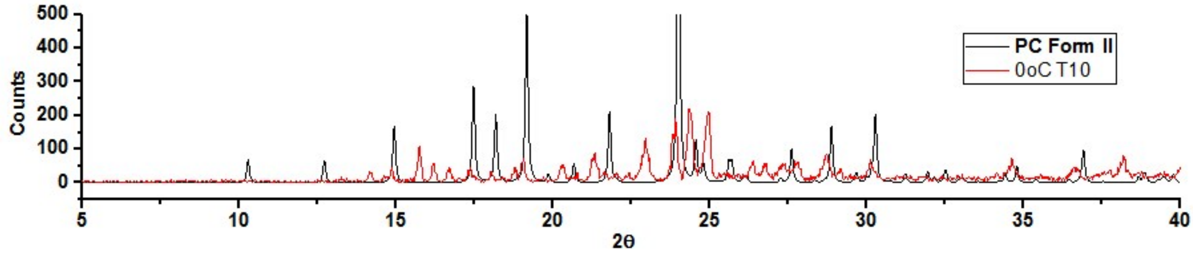
Counts
500
400
300
200
100
0
5
10
15
20
25
30
35
40
2θ
PC Form II
0oC T10

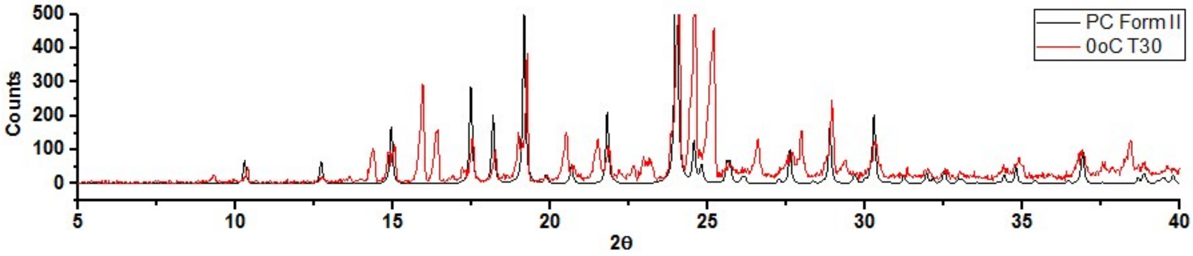
Counts
500
400
300
200
100
0
5
10
15
20
25
30
35
40
2θ
PC Form II
0oC T30

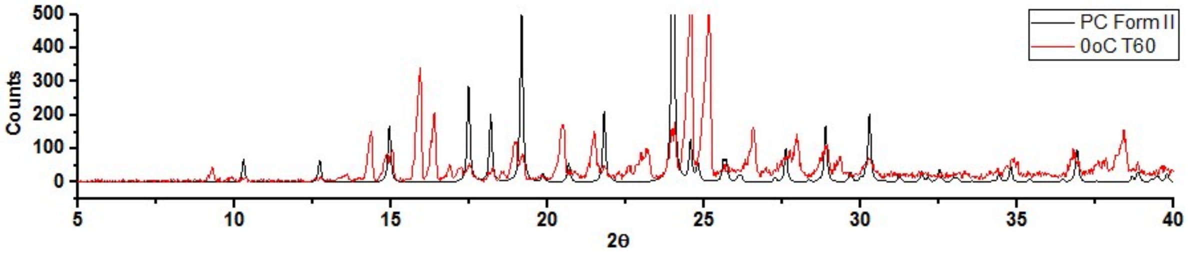

PC Form II
0oC T60
Counts
500
400
300
200
100
0
5
10
15
20
25
30
35
40
2θ

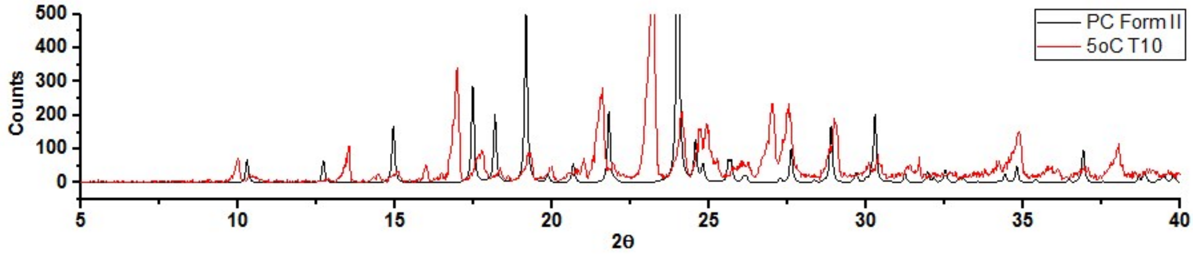

PC Form II
5oC T10
Counts
500
400
300
200
100
0
5
10
15
20
25
30
35
40
2θ

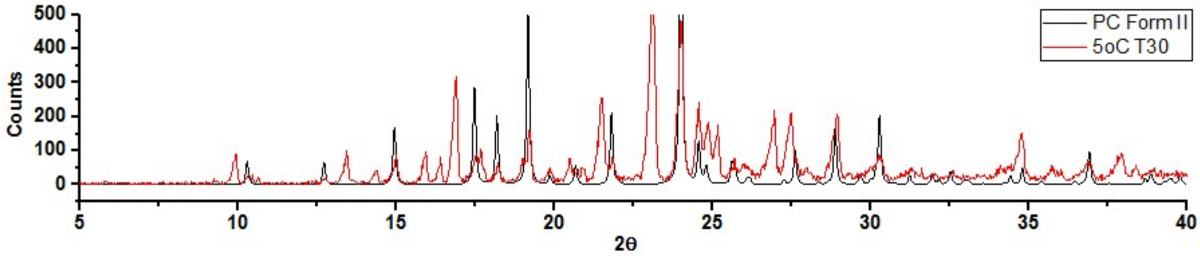

PC Form II
5oC T30
Counts
500
400
300
200
100
0
5
10
15
20
25
30
35
40
2θ

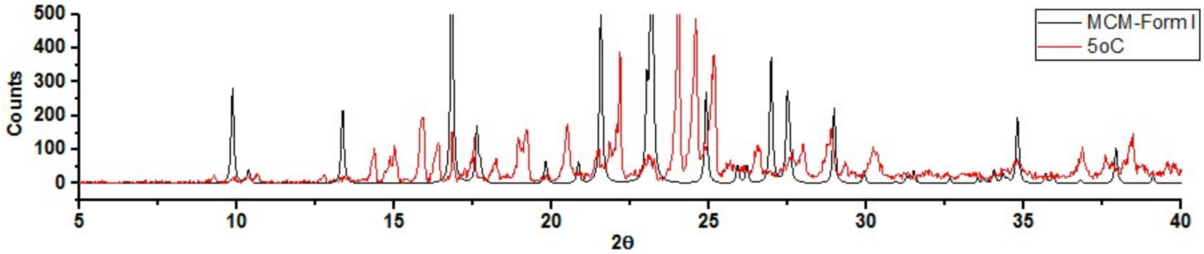

MCM-Form I
5oC
Counts
500
400
300
200
100
0
5
10
15
20
25
30
35
40
2θ

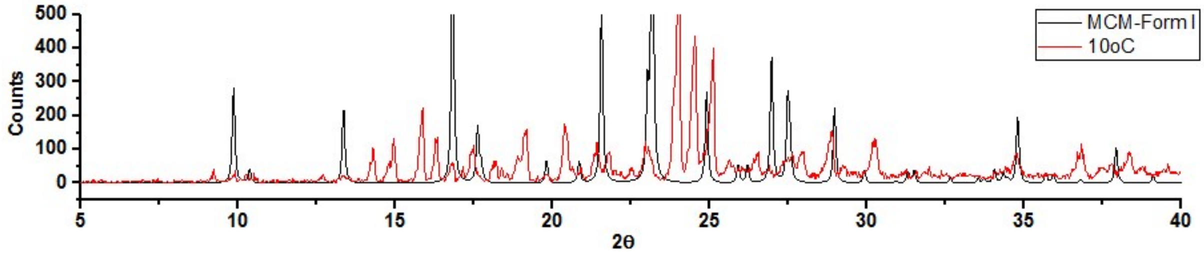

MCM-Form I
10oC
Counts
500
400
300
200
100
0
5
10
15
20
25
30
35
40
2θ

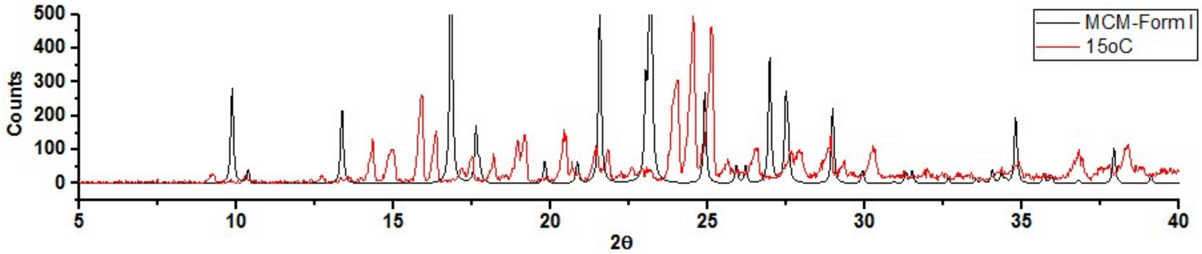

MCM-Form I
15oC
Counts
500
400
300
200
100
0
5
10
15
20
25
30
35
40
2θ

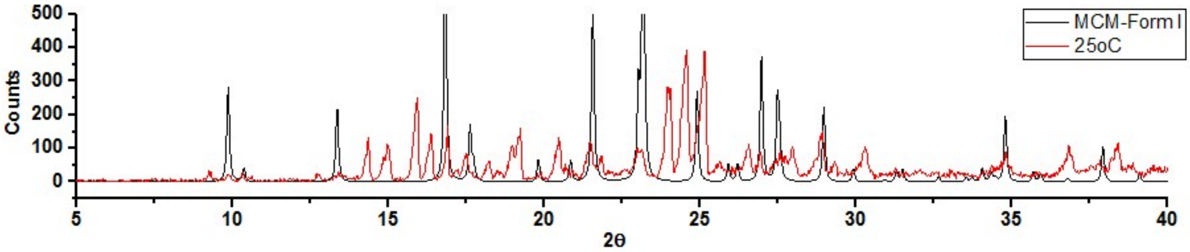

Counts
0
100
200
300
400
500
5
10
15
20
25
30
35
40
2θ
MCM-Form I
25oC

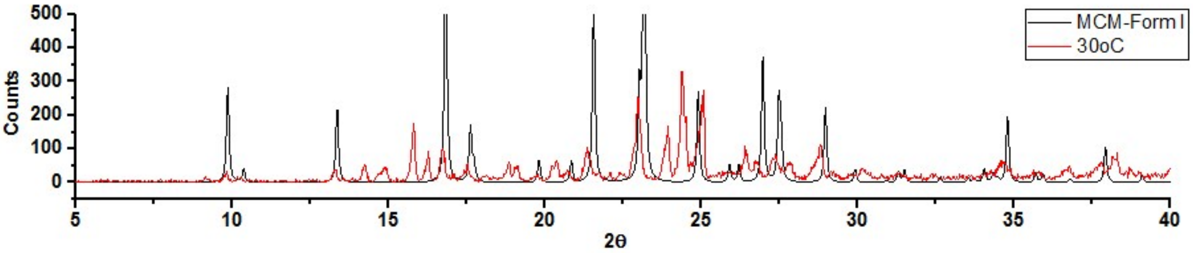

Counts
0
100
200
300
400
500
5
10
15
20
25
30
35
40
2θ
MCM-Form I
30oC

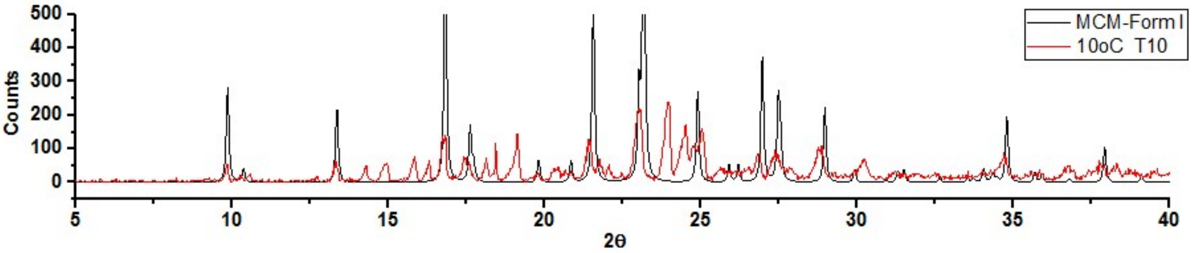

Counts
0
100
200
300
400
500
5
10
15
20
25
30
35
40
2θ
MCM-Form I
10oC T10

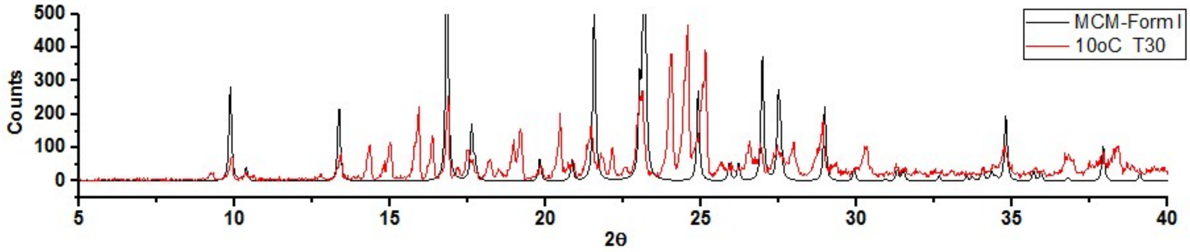

Counts
0
100
200
300
400
500
5
10
15
20
25
30
35
40
2θ
MCM-Form I
10oC T30

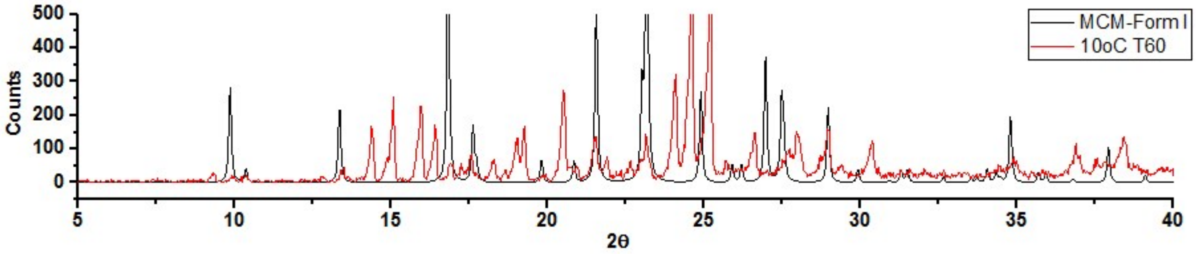

Counts
0
100
200
300
400
500
5
10
15
20
25
30
35
40
2θ
MCM-Form I
10oC T60

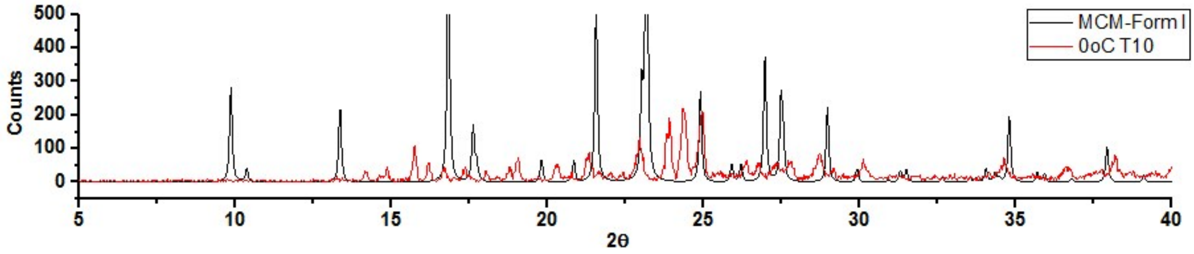

Counts
0
100
200
300
400
500
5
10
15
20
25
30
35
40
2θ
MCM-Form I
0oC T10

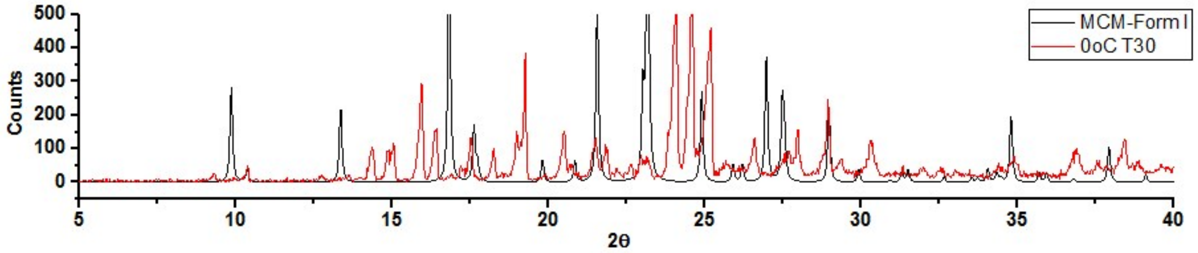
MCM-Form I
0oC T30
Counts
500
400
300
200
100
0
5
10
15
20
25
30
35
40
2θ

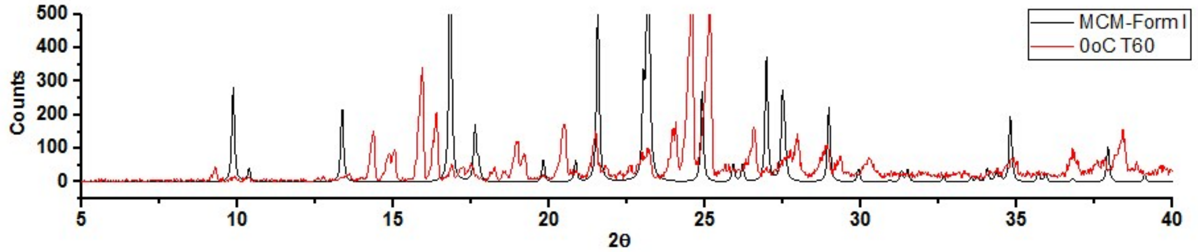
MCM-Form I
0oC T60
Counts
500
400
300
200
100
0
5
10
15
20
25
30
35
40
2θ

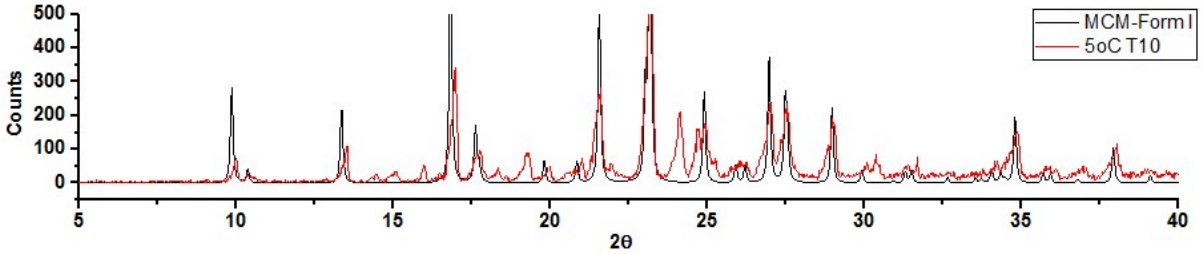
MCM-Form I
5oC T10
Counts
500
400
300
200
100
0
5
10
15
20
25
30
35
40
2θ

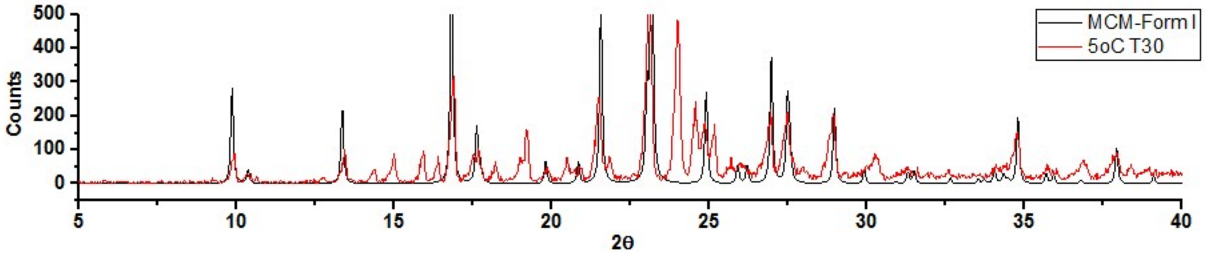
MCM-Form I
5oC T30
Counts
500
400
300
200
100
0
5
10
15
20
25
30
35
40
2θ